Mode evolution of TAE due to alpha particles and synergy with ripple loss in CFETR

Baolong Hao[1,3], Wei Chen[1*], Xiaodong Lin[3], Jiquan Li[1], Guangzhou Hao[1], Jiale Chen[2], Bin Wu[2], Vincent Chan[2], Wenjun Yang[4], CFETR physics team

1. Southwestern Institute of Physics, Chengdu 610041, China
2. Institute of Plasma Physics, Chinese Academy of Sciences, Hefei 230031, China
3. Advanced Energy Research Center, Shenzhen University, Shenzhen 518060, China
4. University of South China, Hengyang 421001, People's Republic of China
5. Advanced Energy Research Center, Shenzhen University, Shenzhen 518060, China

E-mail: chenw@swip.ac.cn

Abstract: The alpha particle should have good confinement when there are instabilities and toroidal field ripple in fusion devices. With the alpha particle slowing down distribution generated by TRANSP/NUBEAM, Alfven eigenfunction calculated by NOVA/NOVA-K, and a quasilinear model in the ORBIT code, the study investigated the nonlinear evolution of Toroidal Alfven Eigenmode (TAE) driven by alpha particles and resulting transport, particularly focusing on the synergistic effect with ripple loss. The amplitude level of strong pulsations is about $A_n = 5.0\times10^{-4} R_0$, frequency chirping and particle transport in phase space are also observed. Enhancement of the saturation level did not occur because the two mode-particle resonant regions are well separated. No synergistic effect of TAE and toroidal field ripple perturbation on alpha particle loss was observed. This is because co-passing particles near the core dominated the mode particle resonance. Only trapped particle redistribution and flattening near the edge can have particle loss enhancement. The conclusions of saturation amplitude, particle transport, and synergy with ripple loss have no concerns for present scenario of CFETR, but no synergy is not a general conclusion and should be investigated case by case. The methodology demonstrated in the work is general and can facilitate rapid iteration of engineering and physics for fusion reactor design.

Keywords: tokamak, alpha particle, TAE, nonlinear dynamics, toroidal field ripple

1. Introduction

The Chinese Fusion Engineering Test Reactor (CFETR) is currently being designed and evaluated for construction. It is a conventional Deuterium-Tritium tokamak, with the goal of conducting burning plasma experiments and achieving tritium self-sufficiency [1-3]. The interaction between Alfven Eigenmodes (AE) and Energetic Particle (EP) is a crucial issue in fusion devices, which is also relevant to astrophysics. The transport properties of alpha particle born with 3.52 MeV in Deuterium-Tritium (DT) reactions determine the success of burning plasma. These properties are crucial for sustaining the fusion process and achieving ignition [4]. Free energy in EP distribution gradient can drive AEs through wave particle resonance, leading to excitation of Alfven instabilities and particle transport [5]. TAE is a predominant type of shear Alfven waves in toroidally confined plasmas and is well studied in experiments [6-8] and theories [9-11]. The linear and nonlinear behavior of AEs and EP transport have been the subject of intense investigation for decades, especially nonlinear dynamics involving mode-mode and wave-particle interactions. There are some reviews that can be referred to, where theoretical formulations and experimental observations are addressed at different times [12-16]. The work on ITER has found EP drive can overcome the thermal ion Landau damping in the outer half of the plasma, with no alpha particle redistribution influencing the fusion burn process in the core region [17-19]. Dedicated experiments during the second JET DT campaign observed TAE excitation driven by alpha particles. Further details on the observation and modeling can be found in Ref. 20.

The complexity and self-organization are inherent characteristics of a burning plasma. One obvious solution is to provide integrated modeling of multiple kinetic-MHD processes, such as micro-turbulence, macroscopic MHD instability, AEs and collisions. This computationally intensive process has been studied using nonlinear gyrokinetic and extended MHD-gyrokinetic simulations, such as GENE [21], GTC [22], MEGA [23] and M3D-K [24], which is costly and can handle spatiotemporal cross-scale interactions. The other solution is to develop a reduced quasilinear model when developing scenarios, whose validity needs to be compared with fully nonlinear simulations and experiments. There are two general paradigms to cope with nonlinear mode-particle interaction: the bump-on-tail and fishbone paradigms [16]. The former description characterizes a system that is close to marginally unstable, where perturbative and EP gyro-radius should be small compared to the mode's radial structure. The mode frequency is mainly determined by equilibrium, with mode amplitude and frequency slowly evolving under EP driving and bulk plasma damping. This is the case with many AEs in tokamak experiments and in this paper [25-27]. When EP effect is non-perturbative and strong enough, the equilibrium and kinetic profiles are significantly modified by mode-particle interactions. The mode function and frequency predominantly evolved due to interactions with EP and continuous spectrum of shear Alfven wave. These interactions enhanced the transport of phase-locked resonant particles and led to the evolution of mode structure. The mode function and frequency are readjusting to maintain phase locking in resonance condition and maximize mode-particle energy exchange [28,29]. This is the case of Energetic Particle driven Mode (EPM), such as fishbone and strongly driven AEs, which can be described by a nonlinear dispersion relation. The general fishbone-like dispersion relation, mainly developed by Chen et al., has several forms in different papers [16, 30]. In general, it has three terms and can be written as $i|s|\Lambda_n = \delta\hat{W}_{nf} + \delta\hat{W}_{nk}$, with Λ_n the generalized inertia term, right-side side have the fluid and kinetic contribution to the potential energy [16]. In Ref. 31, Hao et al. modeled the beam excited fishbones using a general fishbone-like dispersion relation in the EAST experiment [31].

Recent years, there is a new general transport theory of phase space zonal structures, which has been developed for dealing with nonlinear plasma equilibria, Alfven fluctuation spectrum, energetic particle transport and sources/collisions self-consistently. The self-consistent description of phase space zonal structures can cope with multiple spatio-temporal scales and EP transport in phase space. This new approach can deal with nonlinear dynamics of EPM perturbatively and non-perturbatively in energy confinement time scale [32,33]. So, the self-consistent nonlinear evolution of EP driven instabilities should incorporate the mode-mode and mode-particle interactions. The mode-particle nonlinear dynamics dominated the EP driven instability evolution when the perturbation amplitude is relatively low, also known as marginal stability [34].

In reality, it is natural to have a marginally unstable state where the EP population gradually builds up in the presence of sources, sinks and collisions, which is the case of the present paper. A series of papers published after the 1990s by Berk, Breizman and Sharapov have established the bump-on-tail paradigm for AEs nonlinear dynamics [25-27, 35]. For a numerical investigation, White, Chen and Wu have developed a simulation scheme that can handle perturbative excitation and nonlinear evolution of AE, such as amplitude saturation, avalanche, frequency chirping, and resulting EP transport in phase space [36-39]. This perturbative model can provide an efficient and accurate numerical result by making some simplifications, where the mode eigenfunctions are generated by linear stability analysis and kept fixed. The original model was developed by Wu and White with total energy conservation between perturbed magnetic field and perturbed EP distribution [36, 40]. The mode saturation and EP redistribution have been observed from a quiet start [40]. However, the mode frequency modulation is neglected, and only a single toroidal eigenvalue is valid in this method. After that, Chen and White derived the drift kinetic equations in the presence of AEs, and advanced the mode amplitudes and phases over time using a collisional scheme

[39,41]. The model has been continuously improving until recently, incorporating features such as frequency chirping, avalanches due to multiple mode-particle resonance, and EP redistribution with actual NSTX discharge parameters [37, 38].

One fundamental concern in mode-particle interaction is to assess whether significant EP loss occurs, one mechanism is transient loss, also known as convective loss, which happens when resonant particles maintain phase locking with the mode and march out of the loss boundary. The other mechanism is diffusive transport, which occurs due to overlapping resonance and EP stochastic diffusion, receiving many kicks from the instabilities that are decorrelated [29, 42, 43]. Even though there is no particle loss by mode in simulation, the actual situation involves a very effective loss process, which synergizes with mode perturbation and toroidal field ripple. The toroidal symmetry breaking of ripples originates from the discrete nature of toroidal field coils in a tokamak and the complex 3D coil system in a stellarator. The ripple amplitude increases exponentially from the center to the edge, with the maximum value located at the outer midplane. If EP redistribution occurs in a broad region, flattening and broadening the EP profile due to mode-particle resonance can lead to global transport. This phenomenon was observed and modeled for the first time in the TFTR experiment [44], later mentioned in ITER Physics Basis published in 1999 and 2007 [17, 18]. Recently, this problem is incorporated into synergetic effect between internal MHD instabilities and external 3D field, and which confirmed by detailed experiment and analysis in DIII-D [45].

In Ref. 46, Hao et al., conducted a numerical investigation on alpha particle confinement under the perturbations from Neoclassical Tearing Modes (NTM) and ripple in CFETR. The results showed that NTM did not enhance the ripple loss, as no mode-particle resonance was detected in the trapped particle region of phase space, although NTM perturbations and collisions can facilitate a transition between trapped and passing orbits. Only trapped particles experience ripple loss, while passing particles can average the ripple perturbation during their rotational transform orbit. The perturbation amplitude in Ref. 46 is man-made setting and scanned artificially, otherwise, a more self-consistent model of mode evolution and EP transport is presented in this work.

After reviewing the guiding center formalism and mode stepping equations in Section 2, the paper shows plasma parameters, the alpha particle distribution, TAE mode function and ripple loss region of CFETR in Section 3. In Section 4, we present detailed results of the nonlinear evolution of TAE and EP dynamics using ORBIT. Section 5 provides the conclusion and discussion.

2. Mode stepping equation and δf method in guiding center formalism

To carry out TAE excitation and nonlinear evolution, a Hamiltonian guiding center code ORBIT was used in the work. ORBIT has been developed since the 1980s and has been routinely used in physics exploration and experimental analysis [47-49]. The equilibrium, EP distribution and magnetic perturbation can be read numerically in ORBIT or constructed analytically internally. In daily work, the initial distribution and slowing down distribution usually read from TRANSP/NUBEAM [50], Alfven eigenfunction produced by NOVA/NOVA-K [51] and equilibrium read from EFIT [70, 71]. The contravariant representation of axisymmetric equilibrium is $\vec{B} = g\nabla\zeta + I\nabla\theta + \delta\nabla\psi_p$, here ψ_p is the poloidal magnetic flux, θ and ζ are poloidal and toroidal angle coordinates. ORBIT solves guiding center equations in Boozer coordinates, with g, I, and δ are equilibrium functions [49, 52], g and I are the flux functions ψ_p only, δ is the measure of the nonorthogonality of the coordinate system

and can be neglected in guiding center equations of the code. The Hamiltonian is $H_0 = \frac{\rho_{\|}^2 B^2}{2} + \mu B + \Phi$, with $\rho_{\|}=v_{\|}/B$ the normalized particle velocity parallel to the magnetic field, μ the magnetic moment and Φ the electric potential. The plasma rotation in ORBIT could be modeled by creating an electrostatic potential Φ as a function of flux surface. The toroidal and poloidal canonical momenta are $P_\zeta = g\rho_{\|} - \psi_p$, $P_\theta = I\rho_{\|} + \psi$, with ψ the toroidal flux and $q(\psi_p) = d\psi/d\psi_p$ the field line helicity. Variables $\psi_p, \theta, \zeta, \rho_{\|}$ are advanced in time with a fourth-order Runge-Kutta algorithm in ORBIT, using the corresponding Hamiltonian equations [47]:

$$\dot{\theta} = \partial H/\partial P_\theta, \quad \dot{P}_\theta = -\partial H/\partial\theta, \quad \dot{\zeta} = \partial H/\partial P_\zeta, \quad \dot{P}_\zeta = -\partial H/\partial\zeta \qquad (1)$$

The particle orbit in an axisymmetric and time-independent equilibrium is completely determined by the canonical toroidal momentum P_ζ, energy E, magnetic moment μ and direction of parallel velocity. Guiding center equations of motion, including magnetic perturbations, are implemented in ORBIT, and the Hamiltonian with perturbations is $H = \frac{(\rho_{\|} + \alpha)^2 B^2}{2} + \mu B + \Phi$. Two representations of MHD mode read by ORBIT can be expressed as $\delta\vec{B} = \nabla \times (\vec{\xi} \times \vec{B})$ and $\delta\vec{B} = \nabla \times \alpha\vec{B}_0$, with $\vec{\xi}$ the plasma displacement and α a scalar function of position and time [48]. The typical Fourier expansion is $\alpha = \sum_{m,n} A_n \alpha_{mn}(\psi_p) \sin\Omega_{mn}$, where n refers to a single mode with a definite toroidal mode number and frequency ω_n and the sum is done for all poloidal harmonics m with phase $\Omega_{mn} = n\zeta - m_\theta - \omega_n t - \phi_n$. With large aspect ratio approximations, the mode amplitude A_n related with perturbated radial magnetic field is expressed as $\frac{\delta B_r}{B} \simeq \frac{mR}{r} A_n$ [49]. The relation of scalar perturbation α_{mn} with ideal displacement $\vec{\xi}$ can be easily derived with the covariant basis of ideal displacement and equilibrium field, and get an equivalence between the two representations for ideal MHD modes, $\alpha_{mn} = \frac{(m/q - n)}{(mg + nI)} \xi^{\psi}{}_{mn}$, but the scalar perturbation function α_{mn} is more general, as it can also describe resistive modes [49]. For fast ions in ideal MHD modes, the rapid mobility of the electrons makes the electric field experienced by fast ions parallel to the magnetic field equal to zero, so, there must be an artificial electric potential Φ introduced to cancel out the parallel induced electric field generated by $d\vec{B}/dt$. With Fourier expansion of the electric potential Φ and scaler perturbation function α_{mn}, the expression can be derived in Boozer coordinates

$\left(gq+I\right)\omega_n\alpha_{mn}=\left(nq-m\right)\Phi_{mn}$ [53, 54].

The typical analysis of mode-induced loss in ORBIT involves stepping through guiding center equations after reading EP information and mode functions, with the mode amplitude and frequency keeping fixed. At each step, the collision operators for pitch angle scattering and slowing down are considered [55]. The slowing down operator for electron drag of fast ions is given by

$$E_n = E_i - (2\nu_\varepsilon \Delta t)[E_i - (\frac{3}{2} + \frac{E}{\nu_\varepsilon}\frac{d\nu_\varepsilon}{dE})T] \pm 2[TE_i(\nu_\varepsilon \Delta t)]^{0.5} \quad (2)$$

with Δt is the time step, T is the plasma temperature, ν_ε represents slowing down rate, E_n and E_i are particle energy after and before each step. The pitch angle scattering rate from background is given by

$$\lambda_n = \lambda_i(1-\nu_{pa}\Delta t) \pm [(1-\lambda_i^2)\nu_{pa}\Delta t]^{0.5} \quad (3)$$

with ν_{pa} is the pitch angle scattering rate and $\lambda = v_\parallel / v$. For mode evolution, Chen and White have been developing a numerical model in which amplitude and phase are slowly varying [40]. With a perturbation form $\vec{\xi} = \sum_{m,n} An\vec{\xi}_{m,n}(\psi_p)\sin\Omega_{mn}$ and EP current $\vec{J}_{EP} = \int \vec{v}_{EP} f d^3x$, one can derive the following equations within linearized kinetic-MHD formalism.

$$\frac{dA_n}{dt} = -\frac{\nu_A^2}{\omega_n^2 A_n}\left\langle \int \vec{v}_{EP}\cdot\vec{E}_n f d^3x \right\rangle - \gamma_d A_n, \quad (4)$$

$$\frac{d\phi_n}{dt} = -\frac{\nu_A^2}{\omega_n^3 A_n^2}\left\langle \int \vec{v}_{EP}\cdot\partial_t\vec{E}_n f d^3x \right\rangle, \quad (5)$$

which ignoring small term corresponding to $\partial B/\partial t$ [41]. The mode electric filed $\vec{E}_n$ corresponding to plasma displacement is $\vec{E}_n = -\partial_t\vec{\xi}\times\vec{B}$, γ_d is the sum of all damping mechanism from bulk plasma, and ν_A is the Alfven frequency corresponding to bulk plasma density. The distribution of physical EP $f(\psi_p,\theta,\zeta)$ is evaluated in the presence of mode perturbation. $\vec{v}_{EP}\cdot\vec{E}_n$ is the energy transfer between mode and particles, expressed as $\partial_t H = -\rho_\parallel B^2\partial_t\alpha + \partial_t\Phi$. With the Klimontovich representation of Monte Carlo particles

$$f(\psi_p,\theta,\zeta) = \sum_k \delta(\psi_p-\psi_{pk})\delta(\theta-\theta_k)\delta(\zeta-\zeta_k)\Big/N \quad (6)$$

the mode stepping equations can be written as [56]

$$\frac{dA_n}{dt} = -\frac{\nu_A^2}{\omega_n}\sum_{k,m}\left\langle\left[\rho_\parallel B^2\alpha_{mn}(\psi_p)-\Phi_{mn}(\psi_p)\right]\cos(\Omega_{mn})\right\rangle - \gamma_d A_n, \quad (7)$$

$$\frac{d\phi_n}{dt} = -\frac{\nu_A^2}{\omega_n A_n}\sum_{k,m}\left\langle\left[\rho_\parallel B^2\alpha_{mn}(\psi_p)-\Phi_{mn}(\psi_p)\right]\sin(\Omega_{mn})\right\rangle, \quad (8)$$

The normalization factors of particle distribution are implicit in Eq. (7-8), which can be realized by

full-f method to investigate mode-particle interaction non-perturbatively. One of problem in full-f simulation is too much noise from random statistical fluctuations of non-resonant particles, which can be costly. To reduce noise lever, δf method is a common choice because resonant particles only represent a small portion of full distribution. This method can handle situations where mode particle interaction does not change the plasma kinetic profiles significantly. Here, full particle distribution split into equilibrium and perturbation parts, $f = f_0 + \delta f$, and f_0 should be chosen with $\delta f / f_0 \ll 1$. In fusion plasmas, it is natural to choose the steady state classical slowing down distribution as equilibrium distrubiton $f_0(P_\zeta, E, \mu)$, which is a time independent [56]. The perturbed distribution can be expressed as

$$\begin{aligned}\delta f(\psi_p, \theta, \zeta, \rho_\parallel, t) &= \sum_k w_k g(\psi_p, \theta, \zeta, \rho_\parallel, t) \\ &= \sum_k w_k \delta(\psi_p - \psi_{pk}(t))\delta(\theta - \theta_k(t))\delta(\zeta - \zeta_k(t))\delta(\rho_\parallel - \rho_{\parallel k}(t))\end{aligned} \tag{9}$$

with g the numerically advanced marker particles, and w_k the weight function of each particles defined as $w = \dfrac{\delta f}{g}$. Along the orbits, the time derivatives of f and g vanishes, i.e. $df/dt = 0$ and $dg/dt = 0$. To small order of scalar perturbation function α, there is $\dfrac{d\delta f}{dt} = -\dfrac{df_0}{dt} = -\left[\partial_{P_\zeta} f_0 \dot{P}_\zeta + \partial_E f_0 \dot{E} + \partial_\mu f_0 \dot{\mu}\right]$ [41]. Mode-particle interaction is interested in phase mixing within resonant islands, which entails collision-less energy exchange. The magnetic moment μ is conserved for low-frequency instabilities, such as AEs. As a dilute species in the model, EP collisions between EP and bulk plasma are much slower process, primarily reconstructing the original distribution gradient and moving particles in and out of the resonant region. So, the term $\partial_\mu f_0 \dot{\mu}$ is irrelevant to energy transfer and mode evolution for AEs, which can be neglected in the mode stepping equations. The equation for weight stepping along the EP trajectory is given by [37, 38]

$$\frac{dw}{dt} = -\frac{1}{g}\frac{df_0}{dt} = -\frac{f - \delta f}{g}\left[\partial_{P_\zeta} \ln f_0 \dot{P}_\zeta + \partial_E \ln f_0 \dot{E}\right] = (w - w_{t0}) d \ln f_0 / dt \tag{10}$$

where $w_{t0} = \dfrac{f}{g} = \left.\dfrac{f}{g}\right|_{t=0}$ is a constant in time and has conservation properties during mode-particle interaction, $\sum_k w_k = 0$. Here, the initial perturbative distribution is set to zero for a quiet start of mode excitation, and $w_k\big|_{t=0} = 0$ for all particles. Again, the normalization factor corresponding to EP pressure is implicit in weight stepping equations. The marker particle distribution can be chosen arbitrarily, allowing for loading more particles in the resonant region of phase space. Noise from the equilibrium distribution is eliminated in δf method, because it does not contribute to energy transfer between shear Alfven waves and energetic particles. This is because the parallel perturbation fields are too small. Then, terms in the sum

and integral of Eq. (7-8) can be written only with perturbed distribution and have the form

$$\frac{dA_n}{dt} = -\frac{\nu_A^2}{D_n \omega_n A_n} \sum_{k,m} \left\langle w_k \left[\rho_{\|} B^2 \alpha_{mn}(\psi_p) - \Phi_{mn}(\psi_p) \right] \cos(\Omega_{mn}) \right\rangle - \gamma_d A_n , \qquad (11)$$

$$\frac{d\phi_n}{dt} = -\frac{\nu_A^2}{D_n \omega_n A_n^2} \sum_{k,m} \left\langle w_k \left[\rho_{\|} B^2 \alpha_{mn}(\psi_p) - \Phi_{mn}(\psi_p) \right] \sin(\Omega_{mn}) \right\rangle , \qquad (12)$$

with $D_n = 4\pi \sum_m \int \xi_{mn}^2(\psi_p) d\psi_p$ to cope with multiple modes and many poloidal harmonics [37, 38, 56]. Nonlinear mode-mode coupling is completely negligible, but multiple modes can evolve simultaneously through resonant particles in the model.

The marker particle distribution can be chosen to load more particles in the interested region, which requires a high resolution of energy exchange and mode development. In common practice, the initial marker particles are loaded uniformly in phase space or exactly same with equilibrium distribution f_0. But the Klimontovich representation of the general marker particle distribution has too much noise, both the denominator and numerator, $w_{t0} = \frac{f_0(\psi_p, \theta, \zeta, \rho_{\|})}{g_0(\psi_p, \theta, \zeta, \rho_{\|})}$. It is convenient to choose $g_0 = f_0$ to avoid noise in present work, where $w_{t0} = 1$. To further reduce noise in the δf method, marker particles can be limited to regions covering all possible resonance regions. This requires determining resonance before numerically loading marker particles. There are two methods to detect whether there is mode-particle resonance or not, one is to observe the phase vector rotation of test orbit pairs in phase space (P_ζ, E) [57]. The other method is to determine the net energy gain or loss after a sufficient amount of time following the particle.

In weight stepping equation, there are exchange rate of energy $\dot{E}$ and momentum $\dot{P}_\zeta$, free energy in particle gradients $\partial f_0 / \partial$ can only transfer energy with mode through resonance after orbit averaging. There is discrete particle noise in maker distribution during actual discharge analysis, such as sampling particles of steady state slowing down distribution from TRANSP/NUBEAM. The following work will demonstrate a method of spline representation to obtain more precise and general partial derivatives of f_0, where analytical functions are difficult to work, especially for EP distribution during neutral beam heating experiment. Numerical noise is inevitable when stepping particle trajectories in EP code with mode perturbations. White et al. found that making E and P_ζ as primary variables and stepping directly with $(\psi_p, \theta, \zeta, \rho_{\|})$ will result in much better accuracy [58]. The exchange rates of energy and momentum in the weight stepping equation are given by Eq. (13), which have better accuracy of exchange rate of energy $\dot{E}$ and momentum $\dot{P}_\zeta$, which further reduce noise in the model.

$$\frac{dH}{dt} = \partial_t H = -\rho_{\|} B^2 \partial_t \alpha + \partial_t \Phi, \frac{dP_\zeta}{dt} = -\partial_\zeta H = \rho_{\|} B^2 \partial_\zeta \alpha - \partial_\zeta \Phi \qquad (13)$$

3. Distributions of alpha particle, TAE and toroidal field ripple with CFETR parameters

To achieve the facility's goal, the CFETR team developed steady state and hybrid scenarios. We use the plasma parameters from the hybrid scenario (CDM Hybrid 20200330) to investigate the evolution of TAEs and the transport of alpha particles. In this scenario, the target plasma has fusion power about $P_{fus} \approx 1GW$, finite Ohmic flux consumption $\Delta\Phi_{ohm}(4hours) \le 250VS$, $Z_{eff} = 1.9 \sim 2.2$ and plasma density at the pedestal top about 90% of the Greenwald limit. The normalized total plasma beta is about $\beta_N \sim 2.3$. The main engineering parameters of CFETR and other facilities are shown in Table 1, while plasma profiles and magnetic equilibrium are shown in Figs. 1 and 2 (a). The plasma current in this scenario is about 13 MA, and the toroidal magnetic field on axis is about 6.1 T. The steady state classical slowing down distribution of alpha particles is calculated by TRANSP/NUBEAM. The particle density in poloidal cross section is shown in Fig. 2 (a). The collisions with background plasma are included when following marker particles in the work, with typical values of pitch angle scattering rate $\nu_{pa} = 4.5s^{-1}$ and energy slowing down rate $\nu_{\varepsilon} = 0.55s^{-1}$, produced by TRANSP/NUBEAM. Details of sample particle distribution are shown in Fig. 3, which is typical slowing down distributions. The total plasma beta in the center is about $\beta_{therm+EP} \sim 7.3\%$, and the alpha particle beta in the center is about $\beta_{\alpha 0} \sim 1.3\%$.

Table 1. Main parameters of CFETR and other facilities.

Item	CFETR	ITER	HL3	EAST
Toroidal field at the center B_T (T)	6.5	5.3	3	2
Major plasma radius R_0 (m)	7.2	6.2	1.78	1.9
Minor plasma radius a (m)	2.2	2.0	0.65	0.5
Plasma current I_p (MA)	14	15	3	1
Number of TF coils N	16	18	20	16

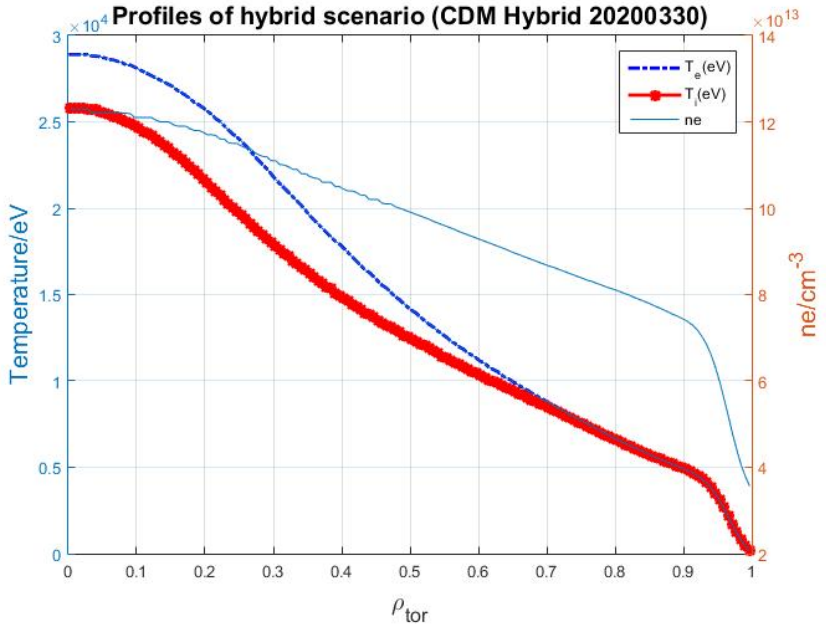

Figure 1. Plasma profiles of electron density (ne), electron temperature (T_e) and ion temperature (T_i) in the CFETR hybrid scenario (CDM Hybrid 20200330).

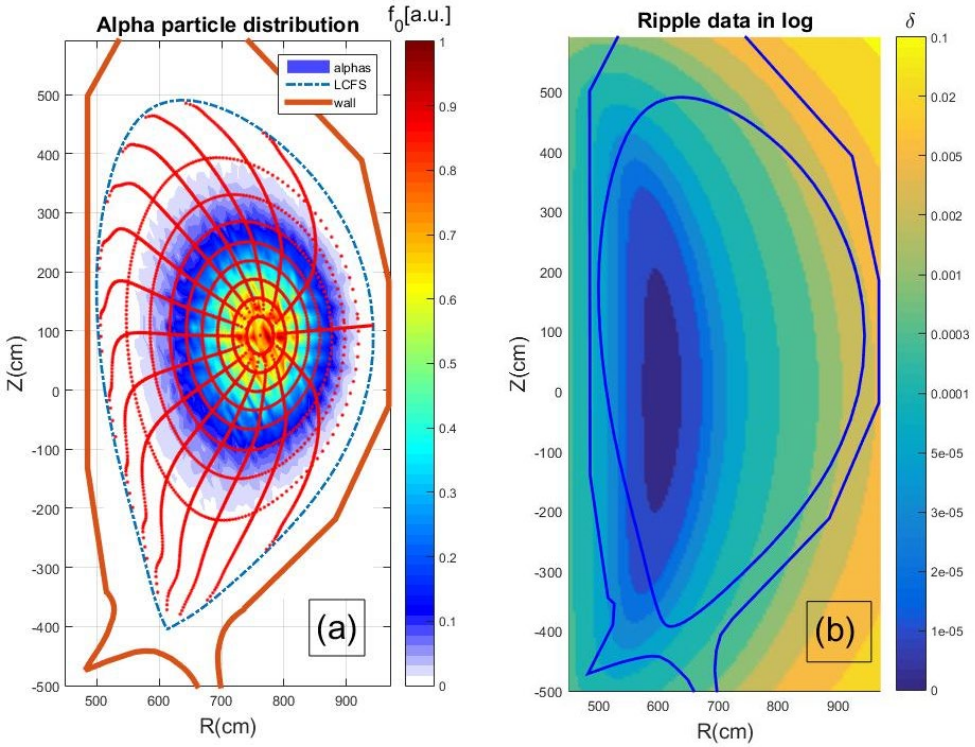

Figure 2. (a) Axisymmetric flux surfaces of equilibrium in Boozer coordinates and slowing down alpha particle density, (b) perturbation amplitude of toroidal field ripple in log-scale from engineering design, Reproduced from [46].

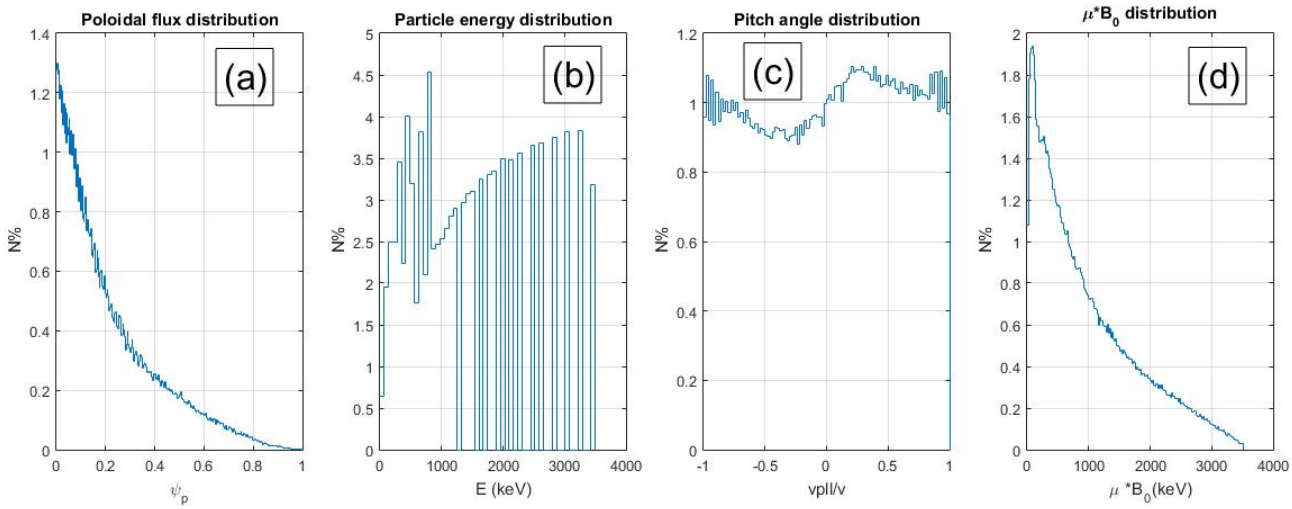

Figure 3. Sample particles generated by TRANSP/NUBEAM, distributions of (a) poloidal flux, (b) particle energy, (c) pitch angle, (d) normalized magnetic moment, unit of Y-axis is the ratio of the number of bin particles to the total number of sample particles.

With equilibrium, plasma profile and alpha particle distribution, the ideal MHD eigenmode is calculated by NOVA/NOVA-K code, which gives an arbitrary mode amplitude and TAE structure, frequency, linear growth rate and damping rate. The effects of finite Larmor radius and finite orbit width are included in NOVA-K. Damping rate is calculated using mechanisms such as electron and ion Landau damping, electron collisional damping, radiative damping and continuum damping. Fig. 4 shows the radial structures of poloidal harmonics of the two most unstable modes, n=7 and n=8 core localized TAE. The frequencies, linear growth rate from alpha particle slowing down distribution, and total damping rates are $f_{n7} = \omega/2\pi = 243.5kHz$, $\gamma_\alpha/\omega = 1.8\%$ and $\gamma_d/\omega = 1.5\%$ for n=7 TAE, $f_{n8} = \omega/2\pi = 274.5kHz$, $\gamma_\alpha/\omega = 3.2\%$ and $\gamma_d/\omega = 2.7\%$ for n=8 TAE. In typical experimental analysis of mode-induced loss with ORBIT and NOVA/NOVA-K, the perturbation amplitude is determined by displacement measurement scaling, such as microwave reflectometer.

Unlike EP distribution with neutral beam injection, which dominantly deposit in the low field side and usually have a single sign of pitch angle, co- or counter-current injection. Fusion born alpha particles have a uniform pitch angle distribution and deposit both on both the low- and high-field side, as shown in Fig. 2 (a) and Fig. 3. To obtain a correct distribution and partial derivatives in phase space $f_0(P_\zeta, E, \mu)$, co- and counter-current moving alpha particles should be loaded at different times, as shown in Figs. 5(a) and (b). Fig. 5(c) shows the ripple loss region for 3.52 MeV alpha particles, produced using the Goldston-White-Boozer (GWB) criterion [59, 60]. The GWB criterion is the critical ripple field perturbation amplitude and widely used for analyzing ripple stochastic threshold, which imposes a more stringent limit on ripple perturbation amplitude compared to ripple well trapping loss. The particle can be ascertained as ripple loss when banana tips of trapped particle located within loss region determined by GWB criterion, and easily extended in phase space [61, 62].

The engineering data of the ripple amplitude distribution in CFETR is shown in Fig. 2 (b). The magnetic field, including ripple perturbation in ORBIT, is expressed as $B(\psi_p, \theta, \phi) = B_0(\psi_p, \theta)[1 + \delta\cos(N\phi)]$, where ripple amplitude δ defined as $\delta(r,\theta) = (B_{\max} - B_{\min})/(B_{\max} + B_{\min})$, with $B_{\max}$ and $B_{\min}$ being the maximum and minimum magnetic field values in the same radial and vertical coordinates in the

poloidal plane [46]. The total field magnitude in ORBIT has been modulated by toroidal field ripple and maintained field divergence free, where a splined file includes equilibrium and ripple field data.

The collisionless ripple stochastic diffusion is the main loss channel for alpha particles in CFETR, as demonstrated in Ref. 46 and 55. If there is an overlap between the dominant alpha particle density and the ripple loss region, there will be a significant ripple loss. Even though there is a slightly increase in particle loss fraction during slowing down, collisions and ripple perturbations can make the orbit transition between passing and trapped. The rapid method to evaluate ripple loss in the plane of $(P_\zeta, \mu B_0/E)$ is reliable [61, 62].

The marker particles, loading to cover all possible resonant regions, can be used to determine the stochastic template in phase space. The work conducts stochastic regions with method of phase vector rotation, as shown in Fig. 6 (a). Phase vector rotation is an effective and accurate method to determine the region of broken Kolmogorov-Arnold-Moser (KAM) surfaces, as illustrated in the plane of (P_ζ, θ), shown in the kinetic Poincare plot of Fig. 6 (b) [46, 57]. Broken KAM surfaces near the plasma edge can result in particle loss, otherwise only local profile flattening occurs. The test orbit pairs of marker distribution, which are located very closely to each other, can rotate constantly within resonant islands. More details of phase vector rotation can be referred to Ref. 57 and 63. Fig. 6 (a) shows the stochastic domains for a small value of μB_0, where the fraction of passing particles is about 73% in the slowing down distribution, as shown in Fig. 3 (d). With a sufficiently large TAE amplitude $A_n = 1\times10^{-3} R_0$, there are dense resonances between TAE and deeply passing particles near the center. The corresponding resonant islands described in Fig. 6 (b), which orbit location along the green line $\omega_n P_\zeta - nE = \text{contant}$ shown in Fig. 6 (a). The initial distribution of test orbit pairs should include all the possible orbit types of alpha particles, especially for counter-moving particles, as described in Fig. 16 of Ref. 46. Time averaged energy transfer between modes and particles is another method to determine the resonance domain in phase space $(P_\zeta, \mu B_0/E)$ or (P_ζ, E). Fig. 6 (c) shows the domain of energy exchange with large amplitude and no collisions, there are many tiny bands of resonance in the center, and the structure of clump and hole in phase space cannot be detected by present resolution. Maker particle in Fig. (c) are load uniformly in phase space to cover all the possible resonant regions. Kinetic Poincare plot corresponding to the green line $\omega_n P_\zeta - nE = \text{contant}$ in Fig. 6 (c) is shown in Fig. 6 (d).

The mode particle resonances exist for both low and high particle energy, and for both passing and trapped particles in the center. Thus, to reduce noise in the mode evolution model, we load marker particles with P_ζ limited only in the work, and found that $P_\zeta/\psi_w \sim$ [-0.4 0.15] for co-moving particles and $P_\zeta/\psi_w \sim$ [-0.6 -0.05] for counter-moving particles are sufficient to cover all the possible resonances, after taking into account the mode structure and density profile of alpha particles. Both the co-moving and counter-moving particles have been investigated in the work. The resonance of counter-moving particles is much less than that of co-moving particles and is barely detected. The following simulation only demonstrates the results of co-moving alpha particles.

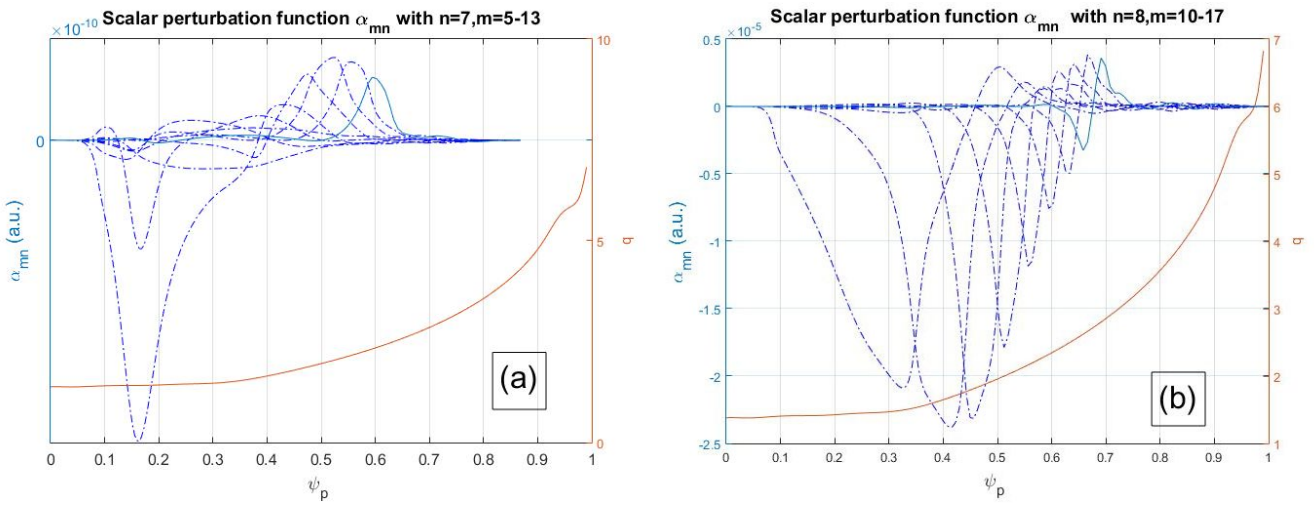

Figure 4. The magnetic potential perturbation of TAE calculated by NOVA/NOVA-K and safety factor q profile, (a) poloidal harmonics of n=7, (b) poloidal harmonics of n=8.

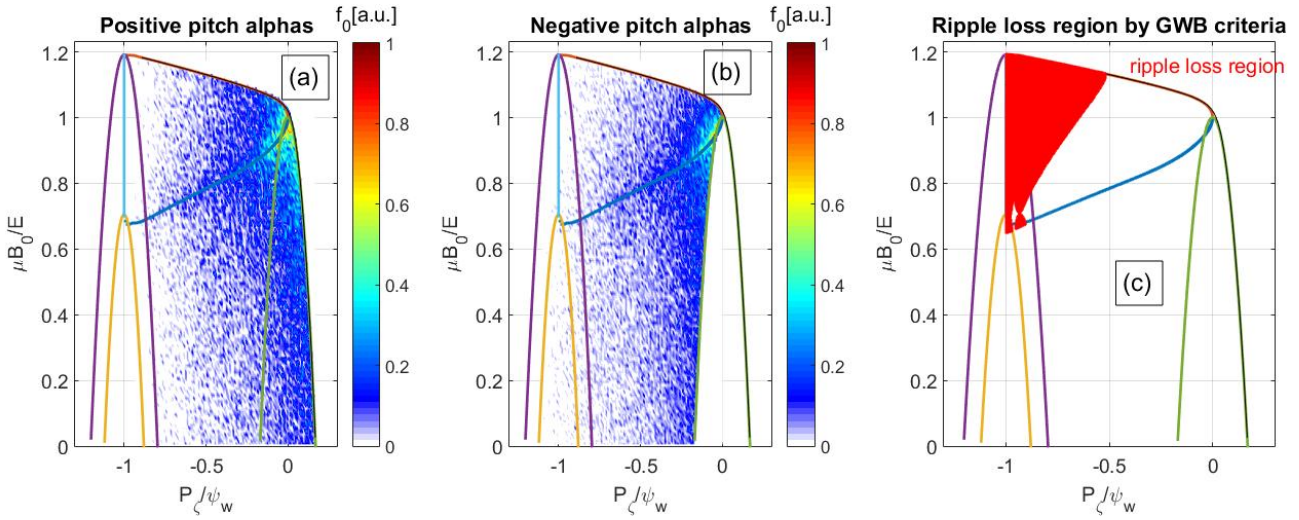

Figure 5. (a) Positive pitch and (b) negative pitch alpha particles in the initial distribution, (c) stochastic ripple diffusion domain determined by GWB criteria with fixed energy $E = 3.52MeV$.

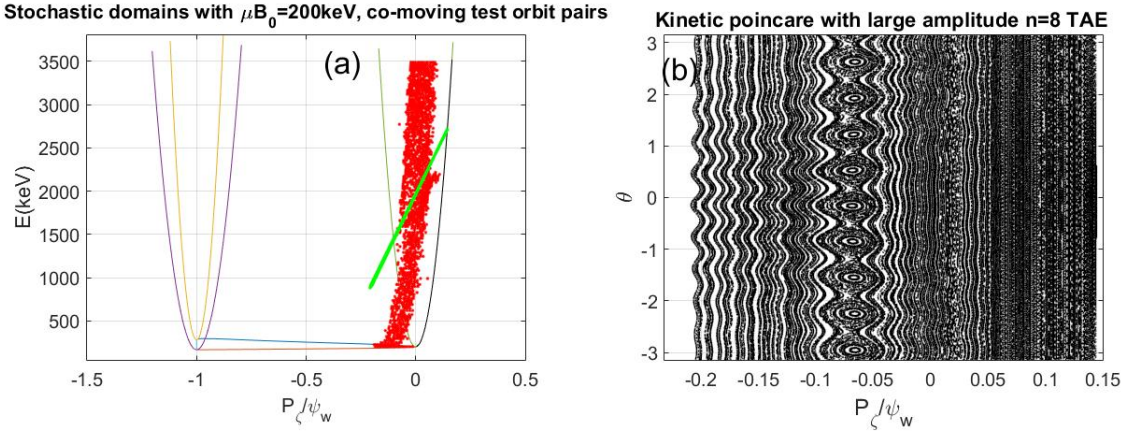

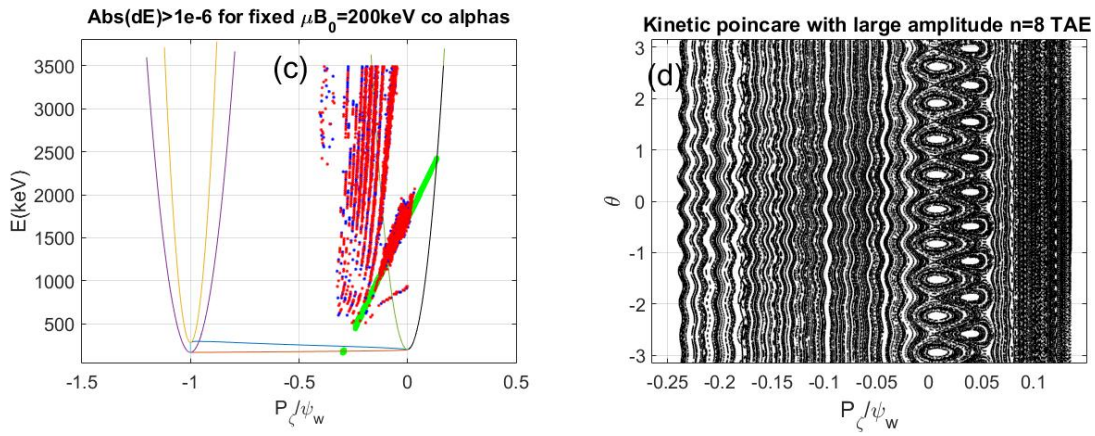

Figure 6. Mode particle resonance with TAE amplitude $A_n = 1.0\times10^{-3} R_0$ and co-moving alpha particles with fixed $\mu B_0 = 200keV$, (a) stochastic template determined by phase vector rotation, (b) kinetic Poincare plot corresponding to particles along the green line $\omega_n P_\zeta - nE = \text{contant}$ in (a). (c) energy transfer dE between TAE and alpha particles calculated with no collisions, red point means energy loss dE/E <-1e-6, while blue point means energy gain dE/E >1e-6, (d) kinetic Poincare plot corresponds to particles along the green line $\omega_n P_\zeta - nE = \text{contant}$ in (c).

Along the orbit of marker particles in perturbed field, partial derivatives of f_0 should be calculated precisely at each step. Unlike the analytical expressions constructed using a slowing-down function or fitted from Monte Carlo codes, this work provides a spline representation that can handle a general case. A list of sampled particles with parameters $(R, Z, v_{\|}/v, E)$ was generated by TRANSP/NUBEAM. Particles with positive pitch angle are read by ORBIT and divided into bins of $f_0(P_\zeta, E, \mu)$, as shown in Fig. 7. A smoother distribution can be obtained by advancing particles with a very small collision rate and short time averaging, then splined representation of two-dimensional Taylor Polynomials $f_0(P_\zeta, E)$ is obtained for each value μ, as demonstrated in Fig. 8. The partial derivatives of $f_0(P_\zeta, E)$ are shown in Fig. 9, which need to invoked during each step of weight function in the simulation.

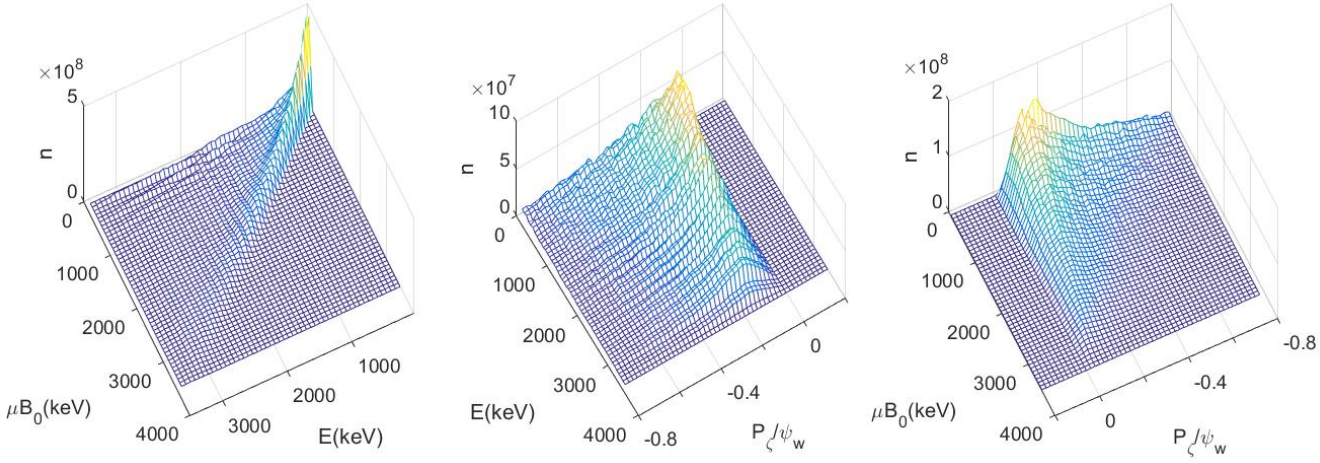

Figure 7. Distribution of sampled particles in bins of (P_ζ, E, μ), read directly from TRANSP/NUBEAM, which involves 160 radial zones and 400 K Monte Carlo ions retained in the slowing down calculation.

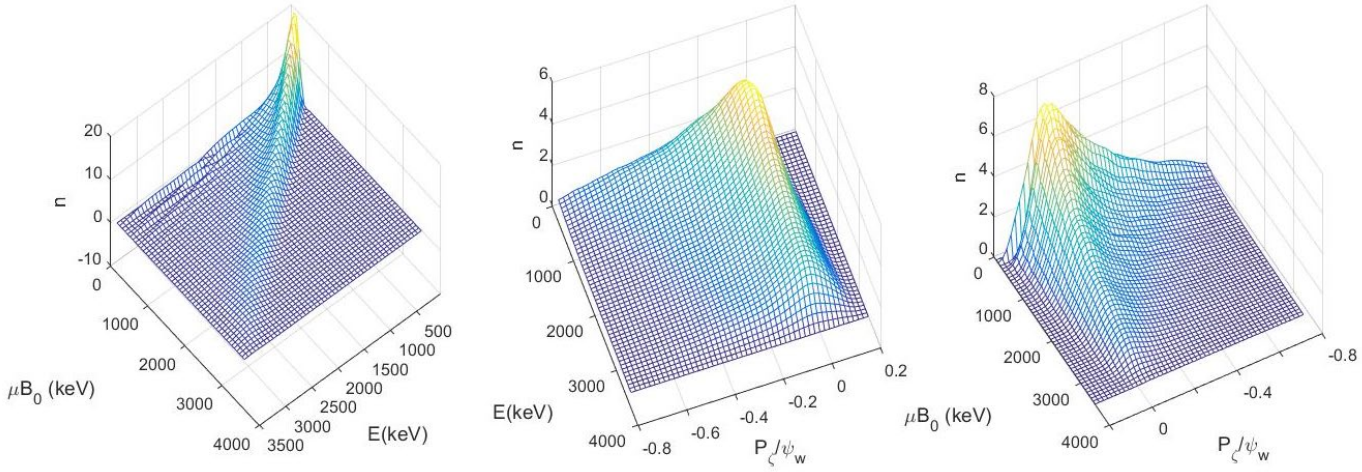

Figure 8. Spline distribution of equilibrium distribution $f_0(P_\zeta, E, \mu)$ in phase space.

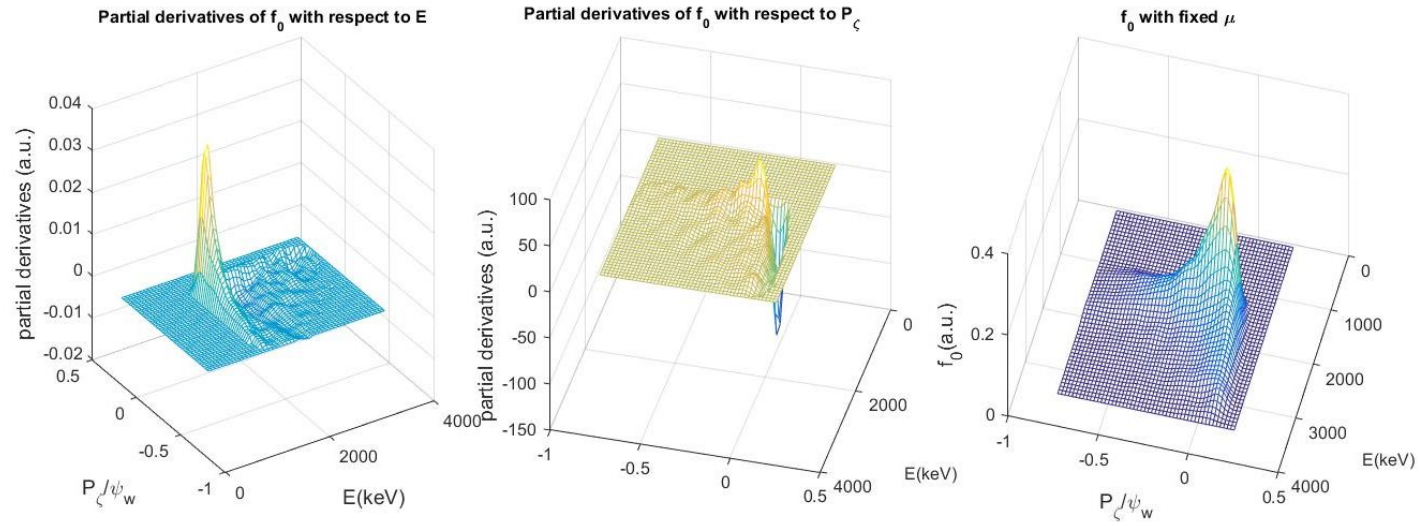

Figure 9. Distribution of partial derivatives $\partial_E \ln f_0$, $\partial_{P_\zeta} \ln f_0$ and equilibrium distribution $f_0(P_\zeta, E, \mu)$ with fixed particle moment $\mu B_0 = 1000keV$.

4. Simulation results of mode evolution and alpha particle transport

With the equilibrium distribution of alpha particles, linear analysis results of TAE and δf scheme described above, we have examined the mode evolution from a quiet start [40, 64]. The initial TAE perturbation amplitude in the calculation is set to a very small value $A_n = 2.0\times10^{-7} R_0$. 370 K marker particles are loaded into ORBIT, covering all the possible resonant region. The mode stepping equations of Eqs. (11) and (12) are advanced 100 times in one toroidal transit, which is typical time for a particle with characteristic energy to move along the magnetic axis toroidally, and is about $3.68\times10^{-6} s$ for 3.52 MeV alpha particle with $v_\parallel / v = 1$. The timescale of the mode step calculation is small enough to observe the

nonlinear weakly driven kinetic instabilities. The evolution of mode amplitude is shown in Fig. 10, alpha particle collisions with background plasma is included in the model, in addition to the drive from gradients of the alpha particle distribution and damping rate. The amplitude level of strong pulsation in Fig. 10 is about $A_n = 5.0\times10^{-4} R_0$, same for both n=7 and n=8 TAE, no particle loss was observed in the simulation. There is no well-defined steady state of saturation amplitude, but rather a periodic modulation, because strong damping rate, weak collisions and localized mode structure, as shown in kinetic Poincare plot of Fig. 6. In general, the collision rate of reactor grade plasma is too small to transport nearby EPs into resonance regions in short time scale here. The work artificially increases collisions in calculations, resulting in more quasi-steady mode saturation and a little larger saturation amplitude.

The frequency chirping is easily observed in present case, which have a large damping rate and small collisions, as shown in Fig. 11 (b). There are small frequency deviations from the eigenfrequency of TAE, coinciding with each amplitude crash, as shown in Fig. 11. With the mode chirping and amplitude crash, the particle density of the phase forms structure of clumps and holes. The redistribution of EP are displayed in Figs. 12 and 13. Fig. 12 (a-c) shows the equilibrium distributions f_0 after integrals, one-dimensional plots of the perturbation distribution $\delta f = w \cdot g$ in case of Fig. 10 (c) are displayed in Fig. 12 (d-f). The results displayed in Fig. 12 (d-f) show the minor modification of alpha particle distribution $\delta f / f_0 \ll 1$ and confirm the marginal stability and perturbative mode-particle dynamics. The initial distribution of marker particles is the same as the equilibrium function f_0, which has been explained in Section 2. Dominant mode particle resonance centers around $P_\zeta / \psi_w \sim -0.07$ for both low and high energies, as shown in Fig. 12 (e), involving passing particles and trapped particles. The location of particle flattening in Fig. 12 (e) confirms the determination of stochastic regions in Fig. 6. Two-dimensional plots of perturbative distribution $\delta f = w \cdot g$ are shown in Fig. 13, which units are same with Fig. 12 in code.

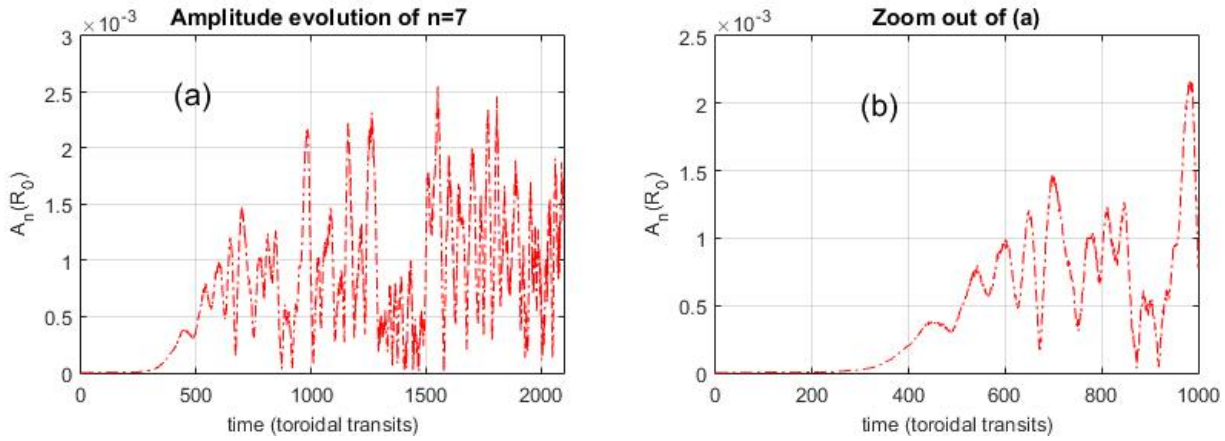

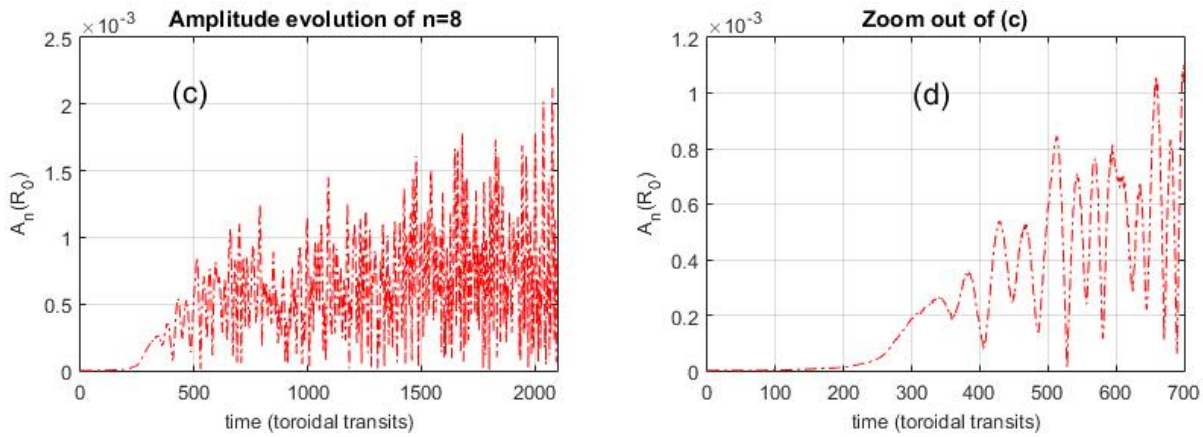

Figure 10. Amplitude evolution with the time unit of one toroidal transit of 3.52 MeV alpha particle on magnetic axis with $v_{\parallel}/v = 1$, (a) and (b) n =7 TAE, (c) and (d) n=8 TAE.

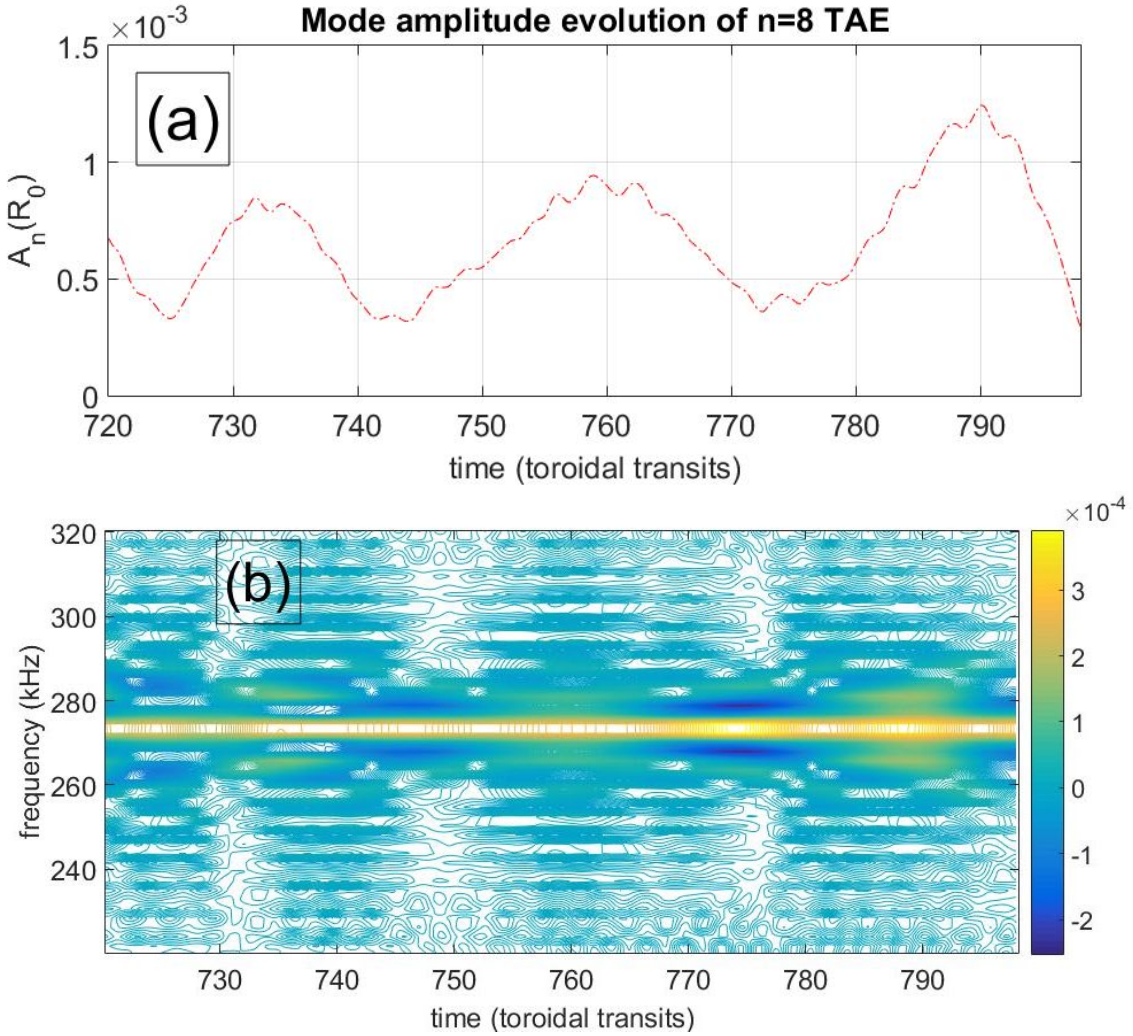

Figure 11. Time evolution of the mode amplitude (a) and frequency spectrum (b) with n=8 TAE.

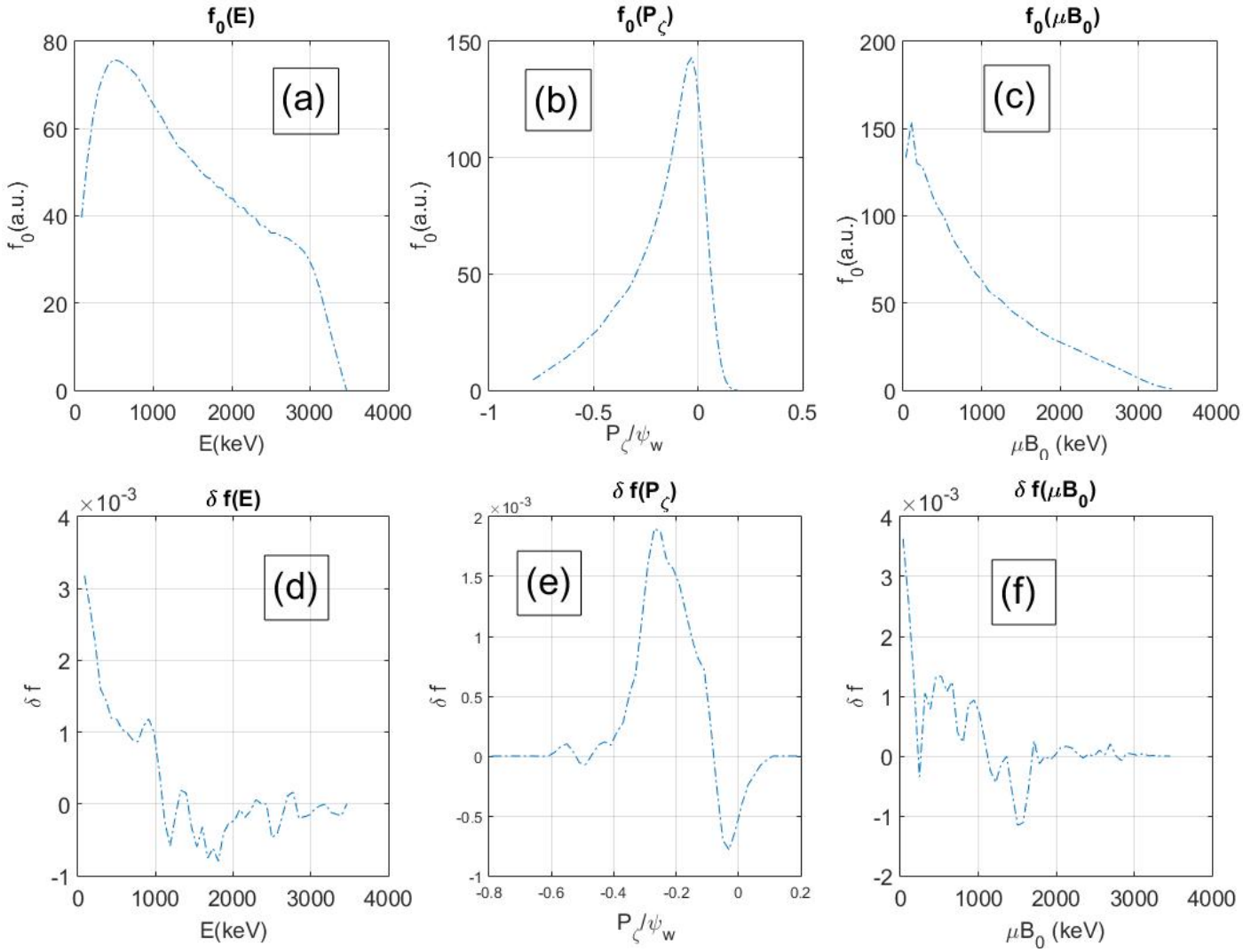

Figure 12. (a-c) Equilibrium distributions f_0 of co-moving alpha particles, (d-f) perturbative distributions $\delta f = w \cdot g$ at the end of the n=8 TAE evolution.

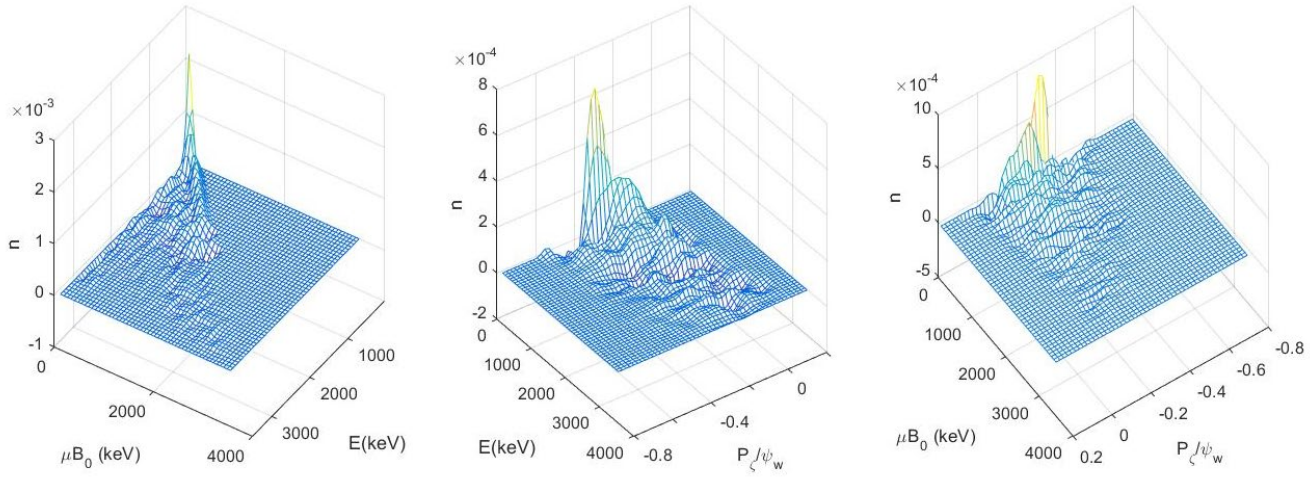

Figure 13. Two dimensional plots of perturbative distribution function $\delta f = w \cdot g$ at the end of n=8 TAE evolution.

There are concerns about mode amplification and resonant island overlap when multiple modes are present. When the mode grows to a large amplitude, particles in isolated and neighboring resonant islands can mix with each other, leading to a broader flattening and further release of more free energy. The criterion for islands overlapping and orbit stochasticity is met when the width of resonance islands exceeds the distance between them [35]. The mode evolution results in Fig. 10 are advanced separately, no mode-mode coupling through resonant particles due to numerical limitations in present ORBIT code. To evaluate the possible multiple modes amplification and global EP redistribution, we calculate the particle diffusion in phase space with TAE perturbations include separately and together, as shown in Fig. 14. A slowing down particle distribution, which means equilibrium distribution f_0, are loaded in the calculation and followed with collisions. $\langle\ \rangle$ means the particle averaged value of difference between each time record and the initial load. For example, $\left\langle dP_\zeta^2 \right\rangle$ equals to $\sum_k^{N_p}(P_{\zeta k} - P_{\zeta k,t=0}) \Big/ N_p$, with $P_{\zeta k}$ is recorded at every ten toroidal transit for each particle, $P_{\zeta k,t=0}$ is the value at the beginning of simulation, N_p is computational particle number. With separated TAE of amplitude $A_n = 5.0\times10^{-4} R_0$, particle diffusion $\left\langle dP_\zeta^2 \right\rangle$ and energy exchange $\left\langle dE^2 \right\rangle$ have the same level for both modes, which means the particle flattening and energy release have the same level. Particle diffusion for both TAE included case is approximately equal to the sum of separated one, as shown in Fig. 14 (a), indicating no resonance overlap in phase space. The detection of resonance by phase vector rotation and energy transfer methods also confirms the conclusion. If there is an enhancement of mode energy from the resonance overlap, the values of $\left\langle dP_\zeta^2 \right\rangle$ and $\left\langle dE^2 \right\rangle$ in the multiple mode case should be four times to that of the separated case, due to the doubling of the resonant island width ΔP_ζ. For single mode particle resonance, resonant particles have $\omega_n \Delta P_\zeta = n\Delta E$. The relation of island width and mode amplitude can be given approximately as $\Delta P_\zeta^2 \propto A_n$. Multimode overlap and amplification have been elaborated by H. L. Berk. If the situation extends to N modes overlapping, then the free energy released to the mode has a factor N^2 due to global flattening [35, 65].

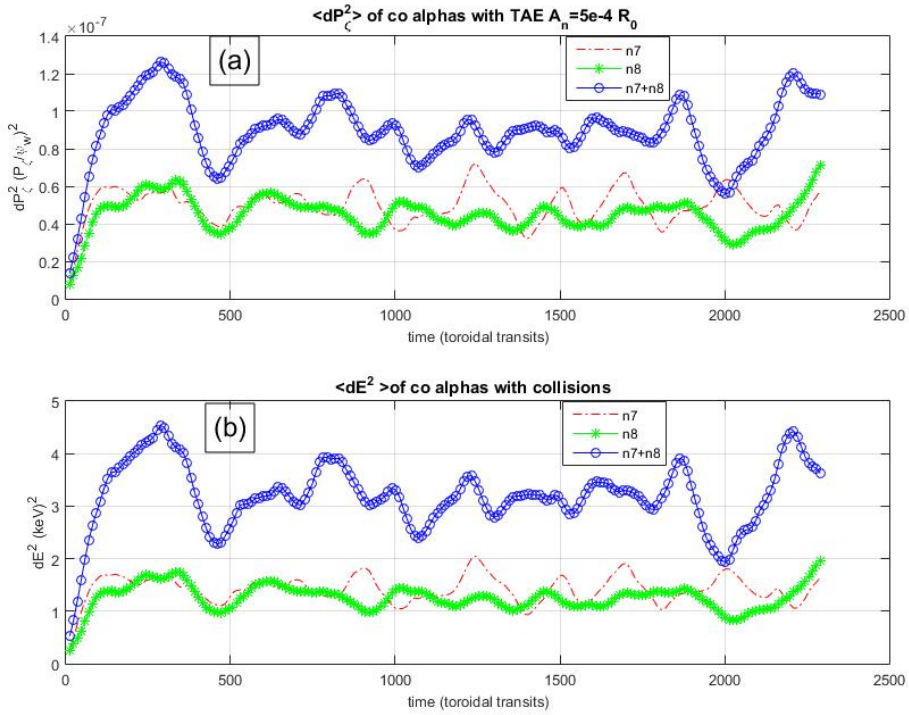

Figure 14. Time history of the mean values of collisional particle diffusion $\left\langle dP_\zeta^2 \right\rangle$ and $\left\langle dE^2 \right\rangle$ with TAE perturbations included separately and together.

5. Synergy analysis of TAE and toroidal field ripple

The local flattening of alpha particles poses a concern regarding the enhancement of ripple loss, which can be quickly evaluated by overlapping particle density with the GWB criterion in the plane of $(P_\zeta, \mu B_0/E)$, as explained in Section 3. The stochastic threshold of GWB criterion to chaotic orbit is determined with given particle energy E. So, it is necessary to determine regions of mode particle resonance in the plane of $(P_\zeta, \mu B_0/E)$, which could be possible with energy transfer method dE. The phase vector rotation originates from the plane (P_ζ, θ) of kinetic Poincare plot, which can only be carried out with particle moment μ fixed and $\omega_n P_\zeta - nE = \text{contant}$, so, it could not be used in the estimation of ripple loss and possible enhancement by TAE.

Fig. 15 shows the time average energy exchange with 200 toroidal transits in the plane of $(P_\zeta, \mu B_0/E)$ with fixed particle energy 3.52 MeV. Co-passing alpha particles near the center dominate the mode particle energy exchange. Resonance and flattening only occur far from the ripple loss region, which shown in Fig. 5(c). Examination of particle density, ripple loss region and local flattening can lead to the conclusion that the synergy between ripple loss and mode-induced particle transport did not occur. Examinations with different particle moment μ have the same conclusion. Quantitative calculation of ripple loss requires following alpha particles for a slowing down time, which is time consuming but accurate. Fig. 16 shows the results of particle loss calculation with TAE and ripple field perturbation separately and together, confirming the absence of synergistic effect. The conclusion of present scenario is not general to CFETR and other fusion reactors, which should be estimated case by case. The synergistic effect between TAE and

ripple is only achieved through the occurrence and overlap of multiple mode-particle resonances from the center to the edge, where ripple loss region located. This leads to significant stochasticity and global transport, which can enhance the particle ripple loss. This diffusion mechanism in high dimensions can be addressed using the stochastic pump model.

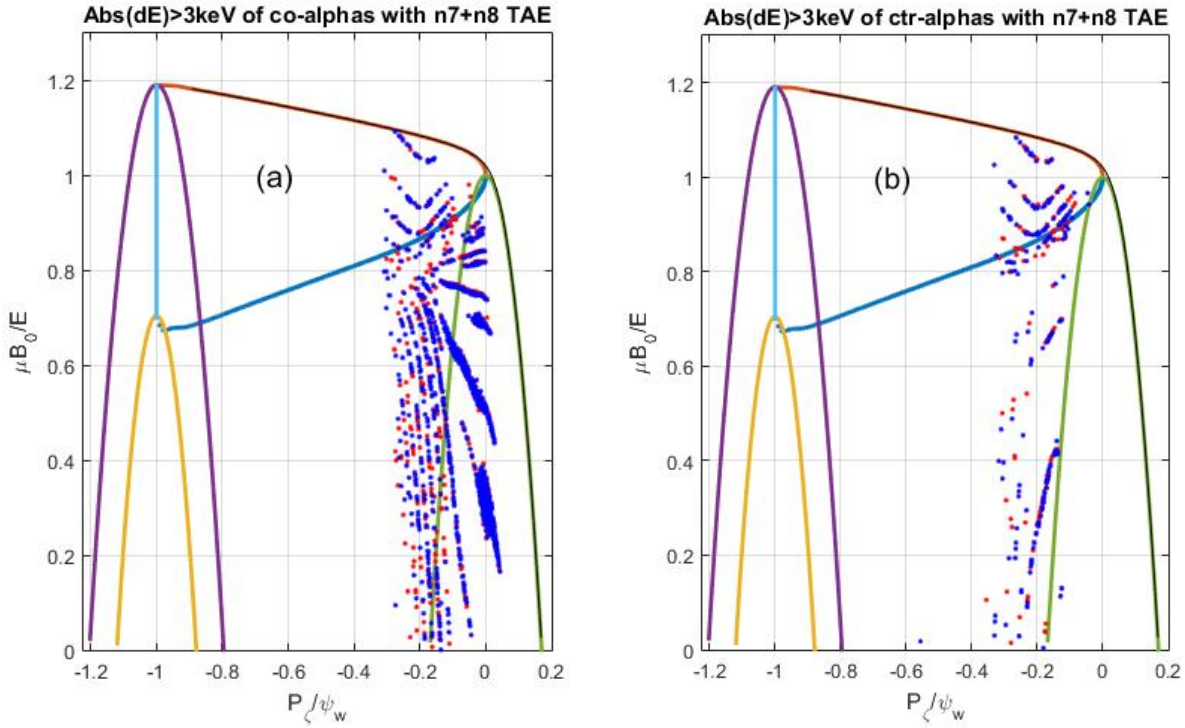

Figure 15. Time averaged energy exchange after 200 toroidal transit times with saturation amplitude $A_n = 5.0\times10^{-4} R_0$. Red points indicate energy loss dE < -3 keV, blue points indicate energy gain dE > 3 keV, (a) co-moving particles, (b) counter-moving particles.

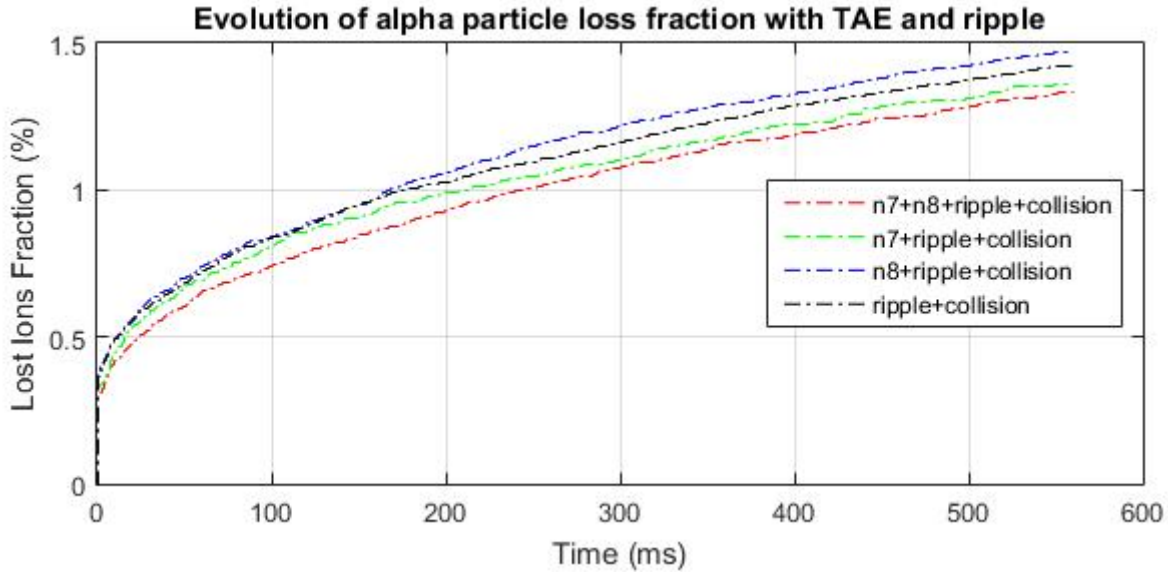

Figure 16. Time dependence of alpha particle loss over one slowing down time, with perturbations from n=7, 8 TAE and toroidal field ripple.

6. Summary and discussion

With the predetermined linear TAE results and alpha particle distribution in CFETR, the paper deals

with the nonlinear evolution of TAE and the associated EP transport in the ORBIT code, particularly focuses on the potential synergistic effect with toroidal field ripple. The spatial structure of TAE perturbation is fixed in the model, while mode amplitude and phase evolve, indicating a perturbative method. Here is the assumption: for a short time-scale compared to the energy confinement time and moderate EP drive, the plasma kinetic profiles do not change significantly [66]. The interaction between mode and particles can be treated with full nonlinear EP dynamics and linear MHD analysis. This implies that the mode structure remains fixed but the amplitude and phase evolve. Nonlinearity originates from the nonlinear dynamics of alpha particles interacting with mode perturbations in a δf method. The work presents several algorithms to reduce noise when calculating marker particle stepping weight, along with two methods to determine resonant regions: phase vector rotation and time-averaged energy transfer. A spline representation of particle distribution in phase space $f_0(P_\zeta, E, \mu)$ has introduced, providing smooth partial derivatives when marker particles move and mode evolve. This representation can be used in actual discharge analysis, such as complicated distribution of auxiliary heating.

TAE driven by alpha particles in CFETR can be treated as weakly driven kinetic instabilities, as the β comparison in Section 3 of the paper. With CFETR parameters and perturbative methods in ORBIT, TAE evolution from a quiet start grows to a pulsation amplitude about $A_n = 5.0\times10^{-4} R_0$. With no mode overlap and global EP transport, the nonlinear evolution of the TAE is observed, including amplitude periodic modulation and frequency chirping. To study the mode overlap effect, particle diffusion $\left\langle dP_\zeta^2 \right\rangle$ and energy exchange $\left\langle dE^2 \right\rangle$ with collisions are examined, and found no multiple resonance overlap. The faster and larger release of free energy from resonance overlap and enhanced stochastic transport of alpha particles did not occur in present scenario. For beam-driven TAE in present tokamak discharge, the collisional particle diffusion is observed to increase with time, as shown in Ref. 67. The $\left\langle dP_\zeta^2 \right\rangle$ diffusion with time was not observed in the work due to collision rate of alpha particles in fusion reactor is much lower than in present EP experiments. Full calculations of particle loss with TAE and ripple perturbations also confirmed that there is no mode overlap and no synergy effect between TAE and ripple, but the conclusion should be given case by case and is not general for CFETR and other fusion reactor [68, 69].

In present work, we have used two methods to determine stochastic regions of mode-particle resonance in phase space. The phase vector rotation is developed from kinetic Poincare plot of the plane (P_ζ, θ), and marker particle orbits must be initiated with fixed μ and $\omega_n P_\zeta - nE = \text{contant}$ [57]. The method of phase vector rotation cannot be used in ripple loss estimation in the plane of $(P_\zeta, \mu B_0/E)$, and method of time averaged energy exchange dE is suitable here. To detect the mode-particle interaction in phase space is a key issue, the Kolmogorov Arnold Moser (KAM) surfaces broken or not determines the EP transport. Ref. 57 has compared three methods, frequency analysis of orbit helicity, fast Lyapunov indicator and phase vector rotation of nearby orbits. In author's practice, the phase vector rotation is more accurate and efficient for detect mode-particle resonance, such as the location, width and overlap of resonance, even for tiny and higher resonance. The rotation rate of orbit pair within islands can give time scale of Landau mixing and transport properties [46].

To quickly evaluate EP transport and possible synergy between ripple and MHD instabilities, one could

examine particle density, ripple loss region, and time-averaged energy transfer of resonant particles in the plane of $(P_\zeta, \mu B_0/E)$, which can provide insights into ripple loss, MHD-induced loss, and synergistic effects resulting from local flattening. The validation of the method has been demonstrated in Ref. 46 and present work. The conclusion provided here and in Ref. 46 have provided confidence that design of CFETR should continue. Investigations of mode-particle interaction with ORBIT have a much faster calculation speed than the gyro-orbit model. However, there are uncertainties in the EP drive when the mode's spatial scale is comparable to the EP gyro-radius, as the EP drive is weakened by orbit averaging. Both models are necessary for fusion reactor design.

Acknowledgements

The first author wishes to acknowledge useful discussions with Roscoe White, Yang Chen, Stephane Ethier, Zhiyong Qiu and Chengyi Song. This work was supported by National Magnetic Confinement Nuclear Fusion Energy Development Project of China (Grant Nos. 2022YFE03070004, 2019YFE03020000), National Nature Science Foundation of China (Grant Nos. 12475216, 12125502, 12475215, 12305240 and 12075155) and Sichuan Science and Technology Program with contract 2023ZYD0016. The work also supported by Innovation Program of Southwestern Institute of Physics (Grants No. 202301XWCX001), Pioneer project of China National Nuclear Power Corporation and China National Nuclear Power Corporation Led the Creation of Scientific Research projects.

References

[1] Chen J., Chan V., Jian X., et al 2021 Integrated modeling of CFETR hybrid scenario plasmas. Nucl. Fusion 61 046002

[2] Chen J., Jia G., Xiang N., 2021 Recent Progress in Modeling of CFETR Plasma Profiles from Core to Edge. Journal of Fusion Energy 40:1

[3] Chen J., Jian X., Chan V., et al 2017 Self-consistent modeling of CFETR baseline scenarios for steady-state operation. Plasma Phys. Control. Fusion 59 075005

[4] Heidbrink W. W., 2002 Alpha particle physics in a tokamak burning plasma experiment. Phys. Plasmas 9 2113

[5] Heidbrink W. W., White R. B., 2020 Mechanisms of energetic-particle transport in magnetically confined plasmas. Phys. Plasmas 27 030901

[6] Nazikian R., Fu G. Y., et al 1998 Toroidal Alfvén eigenmodes in TFTR deuterium–tritium plasmas. 5 1703-1711

[7] Heidbrink W. W., Strait E. J., et al 1991 An investigation of beam driven Alfvén instabilities in the DIII-D tokamak. Nucl. Fusion 31 1635

[8] Wong K. L., 1999 A review of Alfvén eigenmode observations in toroidal plasmas. Plasma Phys. Control. Fusion 41 R1–R56

[9] Fu G. Y. 1995 Existence of core localized toroidicity-induced Alfvén Eigenmode. Phys. Plasmas 2, 1029-1031

[10] Fu G. Y., W. Park 1995 Nonlinear Hybrid Simulation of the Toroidicity-Induced Alfvén Eigenmode Phys. Rev. Lett. 74 1594

[11] Chen L., Zonca F., et al 1998 Nonlinear dynamics of Alfvén eigenmodes in toroidal plasmas. Plasma Phys. Control. Fusion 40 1823

[12] Chen L., Zonca F., 2007 Theory of Alfvén waves and energetic particle physics in burning plasmas. Nucl. Fusion 47 S727

[13] Chen L., Zonca F., 1995 Theory of shear Alfvén waves in toroidal plasmas. Phys. Scr. 1995 81

[14] Gorelenkov N. N., Pinches S. D., and Toi K., 2014 Energetic particle physics in fusion research in preparation for burning plasma experiments. Nucl. Fusion 54 125001

[15] Garcia-Munoz M., Sharapov S. E., et al 2019 Active control of Alfvén eigenmodes in magnetically confined toroidal plasmas. Plasma Phys. Control. Fusion 61 054007
[16] Chen L., Zonca F. 2016 Physics of Alfven waves and energetic particles in burning plasmas. Rev. Mod. Phys. 88 015008
[17] ITER Physics Expert Group on Energetic Particles, Heating and Current Drive 1999 Chapter 5: Physics of energetic ions. Nucl. Fusion 39 2471
[18] Fasoli A., et al 2007 Chapter 5: Physics of energetic ions. Nucl. Fusion 47 S264
[19] Pinches S. D., Chapman I. T., et al 2015 Energetic ions in ITER plasmas. Phys. Plasmas 22, 021807
[20] Oliver H. J., Sharapov S.E., et al 2023 Toroidal Alfvén eigenmodes observed in low power JET deuterium–tritium plasmas. Nucl. Fusion 63 112008
[21] Dorland W., et al 2000 Electron Temperature Gradient Turbulence. Phys. Rev. Lett. 85, 5579
[22] Lin Z., et al 1998 Turbulent Transport Reduction by Zonal Flows: Massively Parallel Simulations. Science 281, 3
[23] Todo Y., Sato T., 1998 Linear and nonlinear particle-magnetohydrodynamic simulations of the toroidal alfvén eigenmode. Phys. Plasmas (1994-present) 5(5), 1321–1327
[24] Park W., et al 1999 Plasma simulation studies using multilevel physics models. Phys. Plasmas 6 1796
[25] Berk H. L., Breizman B. N., 1990 Saturation of a single mode driven by an energetic injected beam. I. Plasma wave problem. Phys. Fluids B 2, 2226–2234
[26] Berk H. L., Breizman B. N., 1990 Saturation of a single mode driven by an energetic injected beam. II. Electrostatic ‘‘universal’’ destabilization mechanism. Phys. Fluids B 2, 2235–2245
[27] Berk H. L., Breizman B. N., 1990 Saturation of a single mode driven by an energetic injected beam. III. Alfvén wave problem. Phys. Fluids B 2, 2246–2252
[28] Heidbrink W. W., 2008 Basic physics of Alfvén instabilities driven by energetic particles in toroidally confined plasmas. Phys. Plasmas 15, 055501
[29] White R. B., Goldston R. J., 1983 Theory of mode induced beam particle loss in tokamaks. Physics of Fluids (1958-1988) 26, 2958
[30] Chen L, White R. B., Rosenbluth M. N., 1984 Excitation of Internal Kink Modes by Trapped Energetic Beam Ions. Phys. Rev. Lett. 52(13), 1122.
[31] Hao B. L., White R. B., et al 2019 Modeling of the beam excited fishbone mode in EAST. Nucl. Fusion 59, 076040
[32] Falessi M. V., Zonca F., 2019 Transport theory of phase space zonal structures. Phys. Plasmas 25, 032306
[33] Bottino A., et al 2022 Time evolution and finite element representation of Phase Space Zonal Structures in ORB5. J. Phys.: Conf. Ser. 2397 012019
[34] Falessi M. V., et al 2023 Nonlinear equilibria and transport processes in burning plasmas. New J. Phys. 25 123035
[35] Breizman, B. N., 2011 Nonlinear Consequences of Energetic Particle Instabilities. Fusion Sci. Technol. 59, 549
[36] Wu, Y., White R. B., Chen Y., Rosenbluth M. N., 1995 Nonlinear evolution of the alpha particle driven toroidicity induced Alfvén eigenmode. Phys. Plasmas 2, 4555
[37] White R. B., Duarte V. N., Gorelenkov N. N., et al 2020 Simulation of Alfvenic avalanche onset in NSTX Phys. Plasmas 27, 022117
[38] White R. B., Duarte V. N., Gorelenkov N. N., et al 2020 Phase-space dynamics of Alfvén mode Chirping. Phys. Plasmas 27, 052108
[39] Chen, Y., White R. B., Fu G. Y., et al 1999 Numerical study of the nonlinear evolution of toroidicity-induced Alfvén eigenmodes. Phys. Plasmas 6, 226.
[40] White R. B., Wu, Y., Chen, Y., et al 1995 Non-linear analysis of the toroidicity induced Alfven eigenmode. Nucl. Fusion 35 1707

[41] Chen, Y., White R. B., 1997 Collisional δ f method. Physics of Plasmas **4**, 3591
[42] Mynick H. E., 1993 Transport of energetic ions by low-n magnetic perturbations. Physics of Fluids B: Plasma Physics 5, 1471
[43] Mynick H. E., 1993 Stochastic transport of MeV ions by low-n magnetic perturbations. Physics of Fluids B: Plasma Physics 5, 2460
[44] White R. B., et al 1995 Toroidal Alfvén eigenmode-induced ripple trapping Phys. Plasmas 2, 2871
[45] Heidbrink W. W., et al 2015 Synergy between fast-ion transport by core MHD and test blanket module fields in DIII-D experiments. Nucl. Fusion 55 083023
[46] Hao B. L., White R. B., et al 2021 Numerical investigation of alpha particle confinement under the perturbation of neoclassical tearing modes and toroidal field ripple in CFETR. Nucl. Fusion 61 046035
[47] White R. B., et al 1984 Hamiltonian guiding center drift orbit calculation for plasma of arbitrary cross section. Phys. Fluids 27 2455-2467
[48] White R. B., Gorelenkov N. N., et al 2010 Particle distribution modification by low amplitude modes. Plasma Phys. Control. Fusion 52 045012
[49] White R. B. 2014 The Theory of Toroidally Confined Plasmas. 3rd edn (Singapore: World Scientific)
[50] Pankin A., et al 2004 The tokamak Monte Carlo fast ion module NUBEAM in the National Transport Code Collaboration library. Computer Physics Communications 159 157
[51] Cheng C., 1992 Kinetic extensions of magnetohydrodynamics for axisymmetric toroidal plasmas. Physics Reports-review Section of Physics Letters. 211. 1-51
[52] White R. B., Boozer A. H., et al 1982 Drift Hamiltonian in Magnetic Coordinates. Phys. Fluids 25 575
[53] White R.B. 2012 Modification of particle distributions by MHD instabilities I Commun Nonlinear Sci Numer Simulat 17 2200
[54] White R.B. 2011 Modification of particle distributions by magnetohydrodynamic instabilities II Plasma Phys. Control. Fusion 53 085018
[55] Hao B. L., Chen W., et al 2021 Numerical simulation of synergistic effect of neoclassical tearing mode and toroidal field ripple on alpha particle loss in China Fusion Engineering Testing Reactor. Acta Phys. Sin., 70(11): 115201
[56] White R. B., et al 2016 Saturation of Alfvén modes in tokamaks. Plasma Phys. Control. Fusion 58 115007
[57] White R. B. 2015 Determination of broken KAM surfaces for particle orbits in toroidal confinement systems. Plasma Phys. Control. Fusion 57 115008
[58] White R. B., et al 2013 Guiding center equations of high accuracy. Plasma Phys. Control. Fusion 55 115002
[59] Goldston R. J., White R. B., Boozer A. H., 1981 Confinement of High Energy Trapped Particles in Tokamaks. Physical Review Letters. 47(9), 647.
[60] Wu B., Hao B. L., White R. B., et al 2017 Calculation of prompt loss and toroidal field ripple loss under neutral beam injection on EAST. Plasma Phys. Control. Fusion 59 025004
[61] White R. B., et al 1996 Ripple-induced energetic particle loss in tokamaks. Phys. Plasmas 3 3043
[62] White R. B., 1998 Chaos in trapped particle orbits. Phys. Rev. E 58, 1774
[63] Hao B. L., et al 2023 Application of high energetic particle redistribution model in CFETR (in Chinese). Nuclear Fusion and Plasma Physics 43(1) 105
[64] Bierwage A., White R. B., Duarte V. N., 2021 On the Effect of Beating during Nonlinear Frequency Chirping. Plasma and Fusion Research 16 1-61
[65] Berk H. L., 2012 Overview of nonlinear kinetic instabilities. AIP Conference Proceedings 1478, 29
[66] Berk H. L., Breizman B. N., et al 1996 Nonlinear Dynamics of a Driven Mode near Marginal Stability. Phys. Rev. Lett. 76 1256
[67] Zhou M. N., White R. B., 2016 Collisional dependence of Alfvén mode saturation in tokamaks. Plasma Phys. Control. Fusion 58 125006

[68] Snicker A., et al 2013 Power loads to ITER first wall structures due to fusion alphas in a non-axisymmetric magnetic field including the presence of MHD modes. Nucl. Fusion 53 093028
[69] Redi M. H., et al 1996 Simulations of alpha particle ripple loss from the International Thermonuclear Experimental Reactor. Phys. Plasmas 3 3037
[70] Fredrickson E.D., et al 2013 Fast-ion energy loss during TAE avalanches in the National Spherical Torus Experiment. Nucl. Fusion 53 013006
[71] Lao L.L., et al 1985 Reconstruction of current profile parameters and plasma shapes in tokamaks. Nucl. Fusion 25 1611